arXiv:1511.05034v2 [cond-mat.mes-hall] 18 Jan 2016

Magnetic Phases of Graphene Nanoribbons under Potential Fluctuations

H. U. Özdemir, A. Altıntaş, and A. D. Güçlü
Department of Physics, Izmir Institute of Technology, IZTECH, TR35430, Izmir, Turkey
(Dated: January 19, 2016)

We investigate the effects of long-range potential fluctuations and electron-electron interactions on electronic and magnetic properties of graphene nanoribbons with zigzag edges using an extended mean-field Hubbard model. We show that electron-electron interactions make the edge states robust against potential fluctuations. When the disorder is strong enough, the presence of electron-hole puddles induces a magnetic phase transition from antiferromagnetically coupled edge states to ferromagnetic coupling, in agreement with recent experimental results.

INTRODUCTION

Graphene[1, 2], a two-dimensional honeycomb lattice of carbon atoms, has been the subject of intense investigation for nanoelectronic and spintronic applications due to its high electric and thermal conductivity, and intrinsic magnetism[3–8]. Although pure graphene is not expected to be magnetic, if the sublattice symmetry of the honeycomb lattice is broken, there is a possibility to induce magnetism[9]. In particular, atomic-scale engineered graphene nanoribbons with zigzag orientation are expected to exhibit magnetized edges with antiferromagnetic coupling between the opposite edges as confirmed by a large number of theoretical literature[10–21] in agreement with Lieb's theorem[9]. However, most likely due to limited control over edge structure in real applications, direct experimental observation is still lacking. Recently, a semiconductor to metal transition as a function of ribbon width was observed in nanotailored graphene ribbons with zigzag edges[22]. This transition is attributed to a magnetic phase transition from the antiferromagnetic configuration to the ferromagnetic configuration, raising hopes for the fabrication of room temperature graphene-based spintronic devices.

The observation of a magnetic phase transition in graphene nanoribbon is a surprising result due to the experimental difficulties for fabricating clean nanostructures with properly passivated and well-defined edges[23–27], and free from imperfections in the lattice or in the substrate. A possible source of irregularity in a graphene structure is the formation of the so called electron-hole puddles[5, 28–30]. Those highly inhomogeneous charge distributions were observed by Martin *et al.*[31] by mapping the charge neutrality point. Later Crommie *et al.*[32] reported that impurities between substrate and graphene sheet induce distorted electron liquid which is in agreement with earlier theoretical works as well[28, 33]. A different study stated that corrugations are the mechanism behind the formation of charge inhomogeneities[34]. On the other hand, it was predicted from tight-binding calculations that the presence of electron-puddles can mask Anderson localization effects favoring metallic behavior[30].

In this work, we investigate the effect of electron-hole puddles resulting from a long-range potential fluctuation on the edge magnetism of finite nanoribbons, using extended mean-field Hubbard calculations. We show that, electron-electron interactions increase the robustness of edge states against disorder as compared to tight-binding approach in finite graphene nanoribbons. More importantly, a transition from antiferromagnetic to ferromagnetic edge phase is observed as the strength of the disorder is increased. These results are consistent with recent experimental observation of semiconductor to metal transition as a function of nanoribbon width[22].

This paper has the following structure. In Section II, we introduce the Hamiltonian model describing the nanoribbon system under investigation, electron-electron interactions, and the long-range potential fluctuation. In Section III, the results including the effects of disorder potential on the electronic properties within the tight-binding and mean-field models are discussed. The antiferromagnetic-ferromagnetic phase transition is investigated in detail for different disorder configurations and interaction strength. Section IV contains a brief summary.

METHOD AND MODEL

Our starting point is a single-band tight-binding model for p_z orbitals, where s, p_x and p_y orbitals are neglected as they mainly contribute to mechanical properties of graphene. Within the mean-field extended Hubbard model, the Hamiltonian is constructed as follows:

$$\begin{aligned} H_{MFH} = & \sum_{i,j,\sigma} (t_{ij} c^{\dagger}_{i,\sigma} c_{j,\sigma} + h.c) \\ & + U \sum_{i} (\langle n_{i,\uparrow} \rangle - \frac{1}{2}) n_{i\downarrow} + (\langle n_{i,\downarrow} \rangle - \frac{1}{2}) n_{i\uparrow} \\ & + \sum_{i,j} V_{ij} (\langle n_j - 1 \rangle n_{i\downarrow} + \langle n_j - 1 \rangle n_{i\uparrow}) \\ & + \sum_{i\sigma} V_{imp}(i) c^{\dagger}_{i\sigma} c_{i\sigma} \end{aligned} \quad (1)$$

First term corresponds to tight-binding approximation where the hopping parameters t_{ij} are taken to be

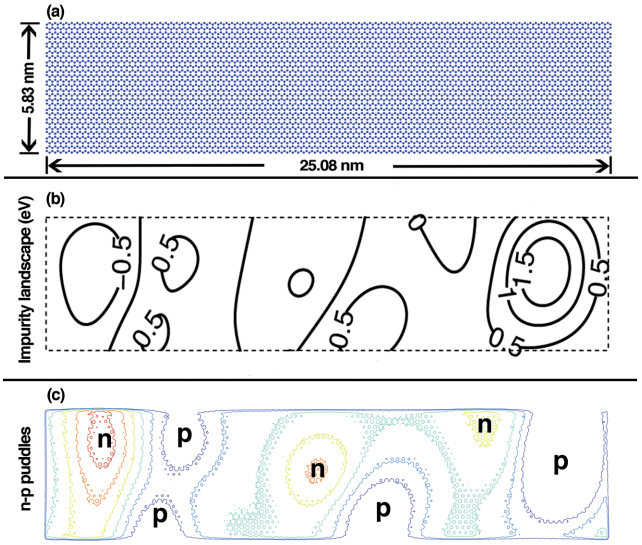

FIG. 1: (Color online) (a) Graphene nanoribbon lattice structure. (b) Randomly generated impurity potential landscape. (c) Total electron density showing the formation of electron-hole puddles (regions denoted by n and p), obtained from mean-field Hubbard calculations

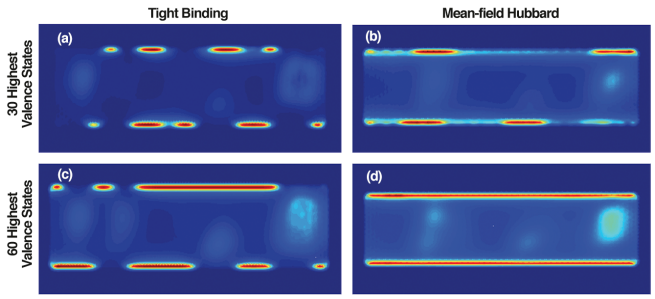

FIG. 2: (Color online) Electronic density profile corresponding to the 30 highest occupied valence states (top panels), and the 60 highest occupied valence states (bottom panels), obtained using tight-binding (left panels) and mean-field Hubbard calculations (right panels). Electron-electron interactions restore the edge states.

$t_{nn} = -2.8$ eV for nearest neighbours and $t_{nnn} = -0.1$ eV for next nearest-neighbours[1]. The operators $c^{\dagger}_{i,\sigma}$ and $c_{i,\sigma}$ create and annihilate an electron at the ith orbital with spin σ, respectively. The terms $\langle n_{i,\sigma} \rangle$ denote the expectation value of electron densities. The second and third terms are onsite and long range Coulomb interaction terms respectively. Here, U is taken to be $16.522/\kappa$ eV, where κ is an effective dielectric constant taken to be as a control parameter. The long-range interaction parameters V_{ij} are taken to be $8.64/\kappa$ eV and $5.33/\kappa$ eV (Coulomb matrix elements are calculated numerically by using Slater π_z orbitals [35]) for the first two neighbors, and $1/d_{ij}\kappa$ for distant neighbors. $V_{imp}(i)$ represents a smooth long-ranged potential fluctuation which can be attributed to charge impurities in the substrate.

Our finite structure contains 5740 atoms respectively giving rise to about 60 edge states. Length of the lattice vectors are $|\vec{a}_{1,2}| = 0.151$ nm. The total length of the ribbon is 25.08 nm and the width is 5.83 nm as shown in Fig. 1a. The mean-field Hamiltonian is solved self-consistently in the subspaces of z-component of the total spin $S_z = (n_{\uparrow} - n_{\downarrow})/2$ (by fixing the number of up and down electrons), and the calculations are performed for several different S_z values (see for instance Fig.5) in order to find the ground state magnetic configuration. Each calculation was repeated several times starting from different initial density matrices to ensure the convergence to a global energy minimum.

Modelling of the long-range electron-hole puddle disorder that can be attributed to charged impurities on structure are carried out with a superposition of Gaussian electrostatic potentials V_{imp} which are randomly distributed over the sample, creating a smooth potential landscape (see Fig. 1b). Impurity potential is given by

$$V_{imp}(i) = \sum_{n} V_n \; e^{-\frac{(\vec{r}_i - \vec{r}_n)^2}{2\sigma^2}} \qquad (2)$$

V_n is the potential peak value (randomly chosen between a minimum and a maximum value) of the nth impurity located at $\vec{r}_n$, σ is the width of the potential which is taken to be 10 times the lattice constant for this study[32]. For such long-ranged scatterers, Anderson localization effects are expected to be suppressed due to the formation of electron-hole puddles[30]. For all calculations a total of 16 impurity sources are used, and the calculations are repeated for randomly generated configurations. Figure 1c shows the formation of electron-hole puddles (i.e. negatively and positively charged regions) in the system calculated by subtracting the positive background charge from the total mean-field electron density.

RESULTS

Before discussing magnetic properties of the nanoribbons, we first focus on the combined effect of long-range potential fluctuations and electron-electron interactions on the electronic properties of edge states. Fig. 2 shows the electronic density profile corresponding to the 30 highest occupied valence states (top panels), and the 60 highest occupied valence states (bottom panels), obtained using tight-binding (left panels) and mean-field Hubbard calculations (right panels), for the disorder configuration given in Fig. 1. We note that in the absence of disorder, valence states include about 30 edge states. In the absence of electron-electron interactions, the main effect of including disorder is to disrupt the edge states, creating highly localized edge states. Note that

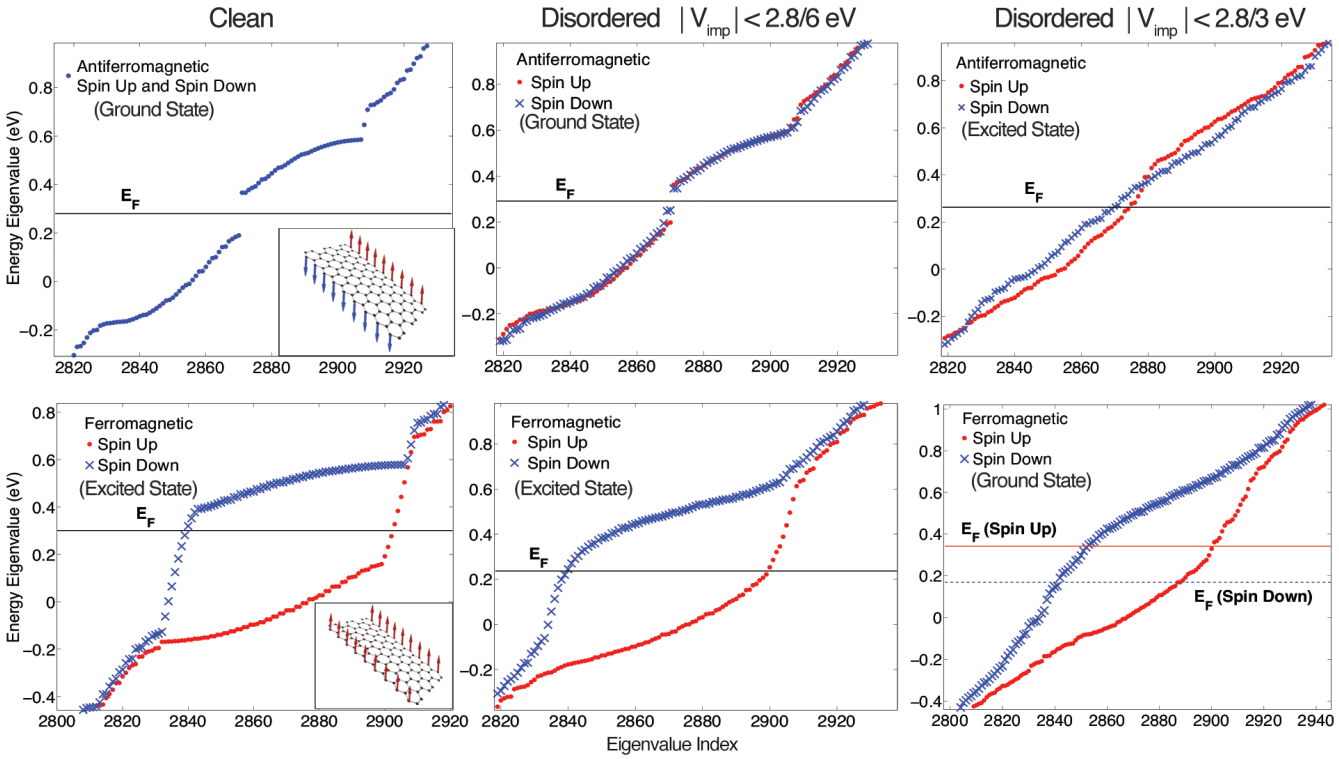

FIG. 3: (Color online) Mean-field Hubbard spectra for antiferromagnetic (top panels) and ferromagnetic (bottom panels) phases, for various degrees of disorder strengths, characterized by V_{imp}. E_F spin up and spin down show the spin-dependent Fermi levels.

the (hole) edge states observed in the tight-binding results are not localized in the p-regions indicated in Fig.1c. Within the extended Hubbard model, however, electrostatically more correct spin-dependent filling order of the edge states is obtained, and the hole edge states close to the Fermi level are now located mostly at the p-regions. Another important effect of electron-electron interactions is that the edges states are recovered within the 60 highest valence states. Thus, electron-electron interactions makes the edge states more robust against disorder by partially restoring the symmetry of the system. Appearance of bulk impurity states is also visible in Fig. 2. An interesting question that arises is how the magnetic properties are affected by the combined effect of disorder and electronic interactions, which we will be the focus of the rest of this work.

In Figure 3, we show the mean-field energy spectra for antiferromagnetic (AFM, top panels) and ferromagnetic (FM, bottom panels) phases, for various degrees of disorder strengths. When no disorder is present, the ground state is AFM and the energy spectrum reveals a gap of the order of 0.17 eV, in agreement with previous theoretical work [10, 22, 36, 37] and recent experimental results[22]. When disorder is included such that $|V_{imp}| < |t_{nn}|/6$, the AFM gap is reduced to 0.1 eV, and the ground state is still AFM. However, when the disorder strength is doubled, the AFM gap is practically closed and the system becomes FM. We note that these results are consistent with the experimental results of Ref.22, where a closing of the gap was observed for ribbon with widths larger than 7 nm, which was attributed to temperature and doping effects. Here we show that, although our system is globally charge neutral, local formation of electron-hole puddles due to long-ranged potential fluctuations can also induce a AFM-FM transition.

The results of Fig. 2 were obtained for the particular disorder configuration shown in Fig.1. In order to check the consistency of the results, we have repeated the calculations for a total of 30 different impurity configurations and strengths. Figure 4a shows the energy difference per atom between the AFM and FM phases, a negative value indicating that the ground state is AFM. For impurity strengths $|V_{imp}| < |t_{nn}|/6$ no significant effect of disorder is observed. However, for $|V_{imp}| < |t_{nn}|/3$, FM phase becomes more dominant. Finally for $|V_{imp}| < |t_{nn}|$, all but one out of ten random impurity configurations give FM ground state. In Fig. 4b we plot AFM spectra energy gaps corresponding to the same configurations in Fig. 4a, showing that the gap quickly decreases as the disorder strength increases.

As discussed earlier, the AFM phase corresponds to $S_z = 0$ and the FM phase corresponds to $S_z = 32$.

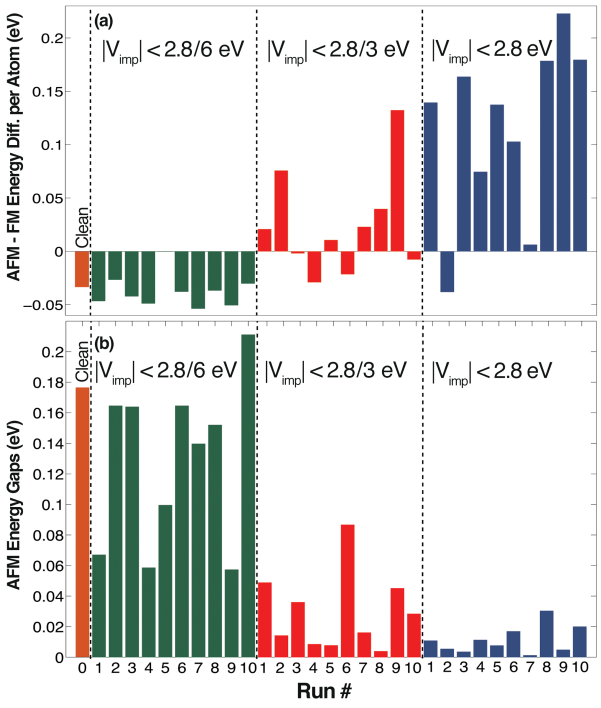

FIG. 4: (Color online) (a) Energy difference per atom between the AFM and FM phases and (b) antiferromagnetic phase energy gap for 30 different disorder configurations with various degrees of disorder strengths. Strong disorder effect causes system to become ferromagnetic. For lower potentials, chance of phase transition reduces.

In order to make sure that no other magnetic phases (which could be due to the presence of electron-hole puddles) were not missed in our calculations we have also performed mean-field calculations for other values of S_z between 0 and 35. Figure 5 shows the total energy of the clean and disordered nanoribbon as a function of S_z, for the disorder configuration shown in Fig.1b. Clearly, within the mean-field approximation, the most important magnetic states that dominate the low energy physics are the AFM and FM phases. We observed similar behavior for other disorder configurations as well.

Up to this point we performed all calculations with $\kappa = 6$ whose value determines the magnitude of electron-electron interaction. As there are three main energy variables in our Hamiltonian, hopping parameter, impurity strength and interaction strength, it is also worth investigating the effect of changing κ. To see the interplay between κ and magnetism, same calculations are performed within $1/\kappa = [0.3, 0.002]$ interval. A convenient way of investigating the AFM phase is to use staggered magnetism which is defined as $(-1)^x(n_{i\uparrow} - n_{i\downarrow})/2$ where x is even for A and odd for B sublattice sites. In Fig. 6, the change of staggered magnetism as a function of dielectric constant is shown. For clean system, no phase transition is observed in this range. On the other hand disordered

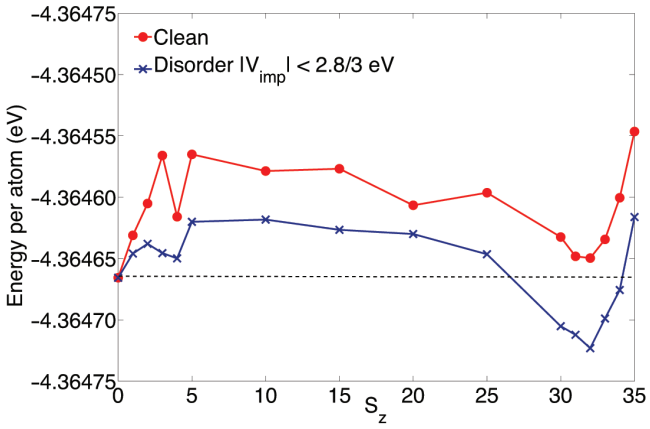

FIG. 5: Total energy of nanoribbon as a function of magnetization S_z. For clean case, the ground state has $S_z = 0$, and for disordered case $S_z = 32$, indicating a FM-AFM phase transition without involving other possible magnetic phases

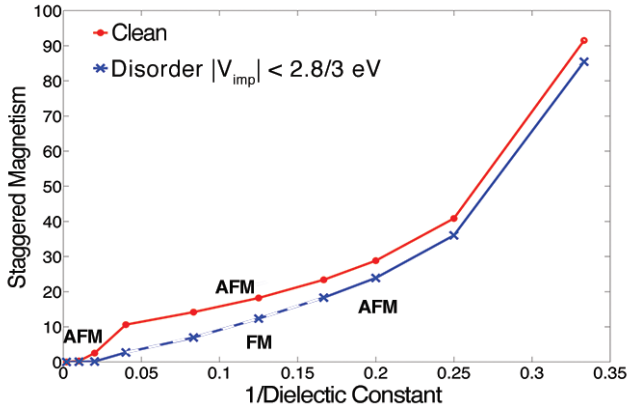

FIG. 6: Staggered magnetism as a function of dielectric constant κ. Clean system (upper line) shows AFM (solid line) coupled edges for all values within $1/\kappa = [0.33, 0.002]$ range. However, FM (dashed line) phase transition occurs between $1/\kappa = [0.167, 0.04]$ after introducing the impurity landscape (lower line). For lower κ values electronic interaction effects become dominant over the impurities hence the system shows AFM phase again.

system shows FM behavior between $1/\kappa = [0.167, 0.04]$. Recovered AFM phase for $1/\kappa > 0.167$ is due to strong electron-electron interactions that suppress the effect of impurities. These results are consistent with our previous results. For $1/\kappa < 0.04$ region magnetic properties can be neglected.

CONCLUSIONS

To conclude, we have investigated the combined effects of electron-electron interactions and random potential fluctuations on the stability of edge states and mag-

netic phases. The electronic stability of edge states is found to be surprisingly robust against disorder due to electron-electron interactions. Moreover, as the disorder potential strength is increased, the system goes through an antiferromagnetic to ferromagnetic phase transition, in agreement with the experimental results of Ref.22. Although the possibility of such a transition is well known from previous calculations[37] for charged system, here the nanoribbon is charge neutral. Thus, the magnetic transition is due to the formation of electron-hole puddles, i.e. local breaking of charge neutrality.

ACKNOWLEDGMENT

This research was supported by the Scientific and Technological Research Council of Turkey TÜBİTAK under the 1001 grant project number 114F331 and by a BAGEP grant from Bilim Akademisi - The Science Academy, Turkey.

[1] A. H. C. Neto, F. Guinea, N. M. R. Peres, K. S. Novoselov, and A. K. Geim, Rev. Mod. Phys. **81**, 109 (2009).
[2] K. S. Novoselov, A. K. Geim, S. V. Morozov, D. Jiang, Y. Zhang, S. V. Dubonos, I. V. Grigorieva, and A. A. Firsov, Science **306**, 666 (2004).
[3] Y.-W. Son, M. L. Cohen, and S. G. Louie, Nature, **444**, 347-349 (2006).
[4] M. Wimmer, I. Adagideli, S. Berber, D. Tomanek, and K. Richter. Phys. Rev. Lett. **100**, 177207 (2008).
[5] J. Bundesmann, M. H Liu, I. Adagideli, and K. Richter, Phys. Rev. B **88**, 195406 (2013).
[6] A. D. Güçlü, P. Potasz, O. Voznyy, M. Korkusinski, P. Hawrylak, Phys. Rev. Lett. **103**, 246805 (2009).
[7] J. Fernandez-Rossier, and J. J. Palacios, Phys. Rev. Lett. **99**, 177204 (2007).
[8] A.D. Güçlü, **arXiv**: cond-mat.mes-hall/1510.05913v1 (2015).
[9] E. H. Lieb, Phys. Rev. Lett. **62**, 1927 (1989).
[10] M. Fujita, K. Wakabayashi, K. Nakada, and K. Kusakabe, J. Phys. Soc. Jpn. **65** (1996).
[11] K. Nakada, M. Fujita, G. Dresselhaus, and M. S. Dresselhaus Phys. Rev. B **54**, 17954 (1996).
[12] O. V. Yazyev, M. I. Katsnelson, Phys. Rev. Lett. **100**, 047209 (2008).
[13] K. Wakabayashi, M. Sigrist, and M. Fujita, J. Phys. Soc. Jpn. **67**, 2089 (1998).
[14] B. Wunsch, T. Stauber, F. Sols, F. Guinea, Phys. Rev. Lett. **101** 036803 (2008).
[15] A. Yamashiro, Y. Shimoi, K. Harigaya, and K. Wakabayashi, Phys. Rev. B **68**, 193410 (2003).
[16] O. V. Yazyev, R. B. Capaz, and S. G. Louie, Phys. Rev. B **84**, 115406 (2011).
[17] H. Feldner, Z. Y. Meng, A. Honecker, D. Cabra, S. Wessel, and F. F. Assaad, Phys. Rev. B **81**, 115416 (2010).
[18] W. L. Wang, O. V. Yazyev, S. Meng, and E. Kaxiras, Phys. Rev. Lett. **102**, 157201 (2009).
[19] J. Cao and S.-J. Xiong, Phys. Rev. B **88**, 085409 (2013).
[20] W. Jaskolski, L. Chico, A. Ayuela, Phys. Rev. B **91**, 165427 (2015).
[21] A. R. Carvalho, J. H. Warnes, and C. H. Lewenkopf, Phys. Rev. B **89**, 245444 (2014).
[22] G. Z. Magda, X. Jin, I. Hagymási, P. Vancsó, Z. Osváth, P. Nemes-Incze, C. Hwang, L. P. Biró, and L. Tapasztò, Nature **514**, 608611 (2014).
[23] X. Zhang, O. V Yazyev, J. Feng, L. Xie, C. Tao,Y. C. Chen, L. Jiao, Z. Pedramrazi, A. Zettl, S. G. Louie, H. Dai, and M. F. Crommie, ACS Nano **7** (1) (2013).
[24] J. Kunstmann, C. Özdoğan, A. Quandt, and H. Fehske, Phys. Rev. B **83**, 045414 (2011).
[25] P. Koskinen, S. Malola, and H. Häkkinen, Phys. Rev. Lett. **101**, 115502 (2008).
[26] P. Koskinen, S. Malola, and H. Häkkinen, Phys. Rev. B **80**, 073401 (2009).
[27] T. Wassmann, A. P. Seitsonen, A. M. Saitta, M. Lazzeri, and F. Mauri, Phys. Rev. Lett. **101**, 096402 (2008).
[28] E. Rossi and S. Das Sarma, Phys. Rev. Lett. **101**, 166803 (2008).
[29] S. Das Sarma, S. Adam, E. H. Hwang, and E. Rossi, Rev. Mod. Phys. **83**, 407 (2011).
[30] G. Schubert and H. Fehske, Phys. Rev. Lett. **108**, 066402 (2012).
[31] J. Martin, N. Akerman, G. Ulbricht, T. Lohmann, J. H. Smet, K. von Klitzing, and A. Yacoby, Nature Physics **4**, 144 - 148 (2008).
[32] Y. Zhang,V. W. Brar, C. Girit, A. Zettl, and M. F. Crommie, Nature Physics **5**, 722 - 726 (2009).
[33] M. Polini, A. Tomadin, R. Asgari, and A. H. MacDonald, Phys. Rev. B **78**, 115426 (2008).
[34] M. Gibertini, A. Tomadin, F. Guinea, M. I. Katsnelson, and M. Polini, Phys. Rev. B 85, 201405(R) (2012).
[35] P. Potasz, A.D. Güçlü, P. Hawrylak, Phys. Rev. B **82**, 075425 (2010)
[36] A. D. Güçlü, M. Grabowski, and P. Hawrylak, Phys. Rev. B **87**, 035435 (2013).
[37] J. Jung, and A. H. MacDonald, Phys. Rev. B **79**, 235433 (2009).